



# Extreme precipitation events induce high fluxes of groundwater and associated nutrients to coastal ocean

Marc Diego-Feliu<sup>1</sup>, Valentí Rodellas<sup>1</sup>, Aaron Alorda-Kleinglass<sup>1</sup>, Maarten Saaltink<sup>2,3</sup>, Albert Folch<sup>2,3</sup>, and Jordi Garcia-Orellana<sup>1,4</sup>

<sup>1</sup>Institut de Ciència i Tecnologia Ambientals, UAB, Bellaterra, E-08193, Spain

<sup>2</sup>Department of Civil and Environmental Engineering, UPC, Barcelona, E-08034, Spain

<sup>3</sup>Hydrogeology Group, UPC-CSIC, Barcelona, E-08034, Spain

<sup>4</sup>Departament de Física, Bellaterra, E-08193, Spain

*Correspondence to:* Marc Diego-Feliu (marc.diego@uab.cat)

**Abstract.** Current Submarine Groundwater Discharge (SGD) studies are commonly conducted under aquifer baseflow conditions, neglecting the influence of episodic events that can significantly increase the supply of nutrients and water. This limits our understanding of the social, biogeochemical, and ecological impacts of SGD. In this study, we evaluated the influence of an extreme precipitation event (EPE) on the magnitude of both the terrestrial and marine components of SGD. To do so, three seawater sampling campaigns were performed at a Mediterranean ephemeral stream-dominated basin after an extreme precipitation event (~90 mm in few hours) and in baseflow conditions. Results indicate that the groundwater flows of terrestrial and marine SGD after the extreme precipitation event were 1 order of magnitude higher than those in baseflow conditions. SGD induced by extreme precipitation events, which only take place a few days per year, represented up to one third of the annual discharge of groundwater and associated nutrients at the study site. This work accentuates the need to account for episodic increases in the supply of water and nutrients when aiming at providing reliable annual SGD estimates, particularly in the current context of climate change, since the occurrence of such events is expected to increase worldwide.

## 1 Introduction

Submarine groundwater discharge (SGD) - the flow of terrestrial and marine groundwater to the coastal ocean - is one of the primary processes regulating the transfer of solutes from land to ocean (Santos et al., 2021). The significance of this process at local, regional and global scale stems mainly from its role in modulating the water and chemical budgets of oceans, controlling coastal ecosystems, and contributing to the well-being of coastal societies (Alorda-Kleinglass et al., 2021; Lecher et al., 2015; Luijendijk et al., 2020). In the last three decades, there have been many studies focusing on quantifying SGD and associated solute fluxes in multiple sites across the globe, including coves, bays, estuaries, and entire basins (e.g., Beck et al., 2008; Kwon et al., 2014; Tamborski et al., 2020). However, most of the SGD investigations are conducted under baseflow conditions, that is, in the absence of any meteorological, hydrological, or oceanographical event (e.g., storms, monsoons, sea-



level anomalies) which might significantly impact the magnitude of SGD. Only a few articles have focused on the evaluation of the temporal variations in SGD induced by episodic events (Adyasari et al., 2021; Gonnee et al., 2013; Hu et al., 2006; Rodellas et al., 2020; Sugimoto et al., 2016). Extrapolating from SGD estimates derived under baseflow conditions to obtain annual fluxes neglects the role of such events, which may represent an important contributor to overall SGD fluxes.

Extreme precipitation events (EPE) represent one of the main natural hazards producing severe societal and economic costs in urban, agricultural, and mountainous areas (Booij, 2002; Camarasa-Belmonte and Soriano-García, 2012; Schumacher, 2017). The meteorological causes of these events include the formation of cyclones, fronts, monsoons, isolated thunderstorms, upslope flow precipitation, and others, and vary from region to region (Kunkel et al., 2012). The social and environmental consequences also vary geographically and depend on diverse aspects such as topography, soil characteristics, geological setting, land surface use and characteristics, and human-induced changes to the landscape and coastal areas (Schumacher, 2017). Due to the disparate causes and consequences associated with them, there are different ways for defining an ‘extreme’ precipitation event: some authors define such events as those exceeding an arbitrary threshold of 24h-accumulated rainfall (e.g., Lionello et al., 2006; Meenu et al., 2020); others use the 90<sup>th</sup>, 95<sup>th</sup>, or 99<sup>th</sup> all-day or wet-day percentile (Pendergrass and Knutti, 2018). Whilst episodic increases in surface runoff linked to EPE are often well characterized (e.g., Camarasa-Belmonte and Tilford, 2002; Moore, 2007; Rajurkar et al., 2004), little is known about the influence of EPE on SGD-driven water flows and associated solute fluxes to the coastal ocean. Extreme precipitation events may indeed promote aquifer recharge through the infiltration of rainwater (Ramos et al., 2020; Yu et al., 2017), although its effects on piezometric levels (quantitatively and temporally) depend on several factors, such as soil composition, geological characteristics, the hydraulic parameters of the aquifer, and others. Infiltrated water displaces groundwater stored in the aquifer towards the sea, enhancing mixing processes in the coastal aquifer (Anwar et al., 2014; Palacios et al., 2019; Robinson et al., 2018). The significance of EPE on SGD may be exacerbated in areas subject to an arid or semi-arid climate, with scarce and unevenly distributed precipitation, and where extreme events may be the only form of recharge for the aquifer (Taylor et al., 2013). Understanding the role of EPE on SGD-driven water flows and associated solute fluxes is thus fundamental in order to (1) accurately constrain annual fluxes of any dissolved compound transported by SGD, (2) integrate episodic-induced SGD in global estimates, (3) evaluate the environmental impacts of these episodic events on coastal ecosystems and (4) foresee the role of SGD in the future climate change scenario.

This study evaluates the significance of SGD and the associated nutrient fluxes induced by EPE in a Mediterranean coastal zone, the implications of neglecting EPEs on annual estimates, and its importance in the context of climate change. The study was conducted at a typical Mediterranean ephemeral stream-dominated basin. These areas are characterised by rapid response to precipitation due to their geomorphological features (small catchment areas, sharp slopes, coastal alluvial aquifers, and sporadic surficial torrential courses; Camarasa-Belmonte and Segura Beltrán, 2001) and thus represent an ideal setting for gauging the influence of such events.



## 2 Methods

### 65 2.1 Study site

Maresme County is a coastal region located to the NE of the city of Barcelona (Spain, western Mediterranean Sea) that extends from the Catalan Littoral Mountain Range to the Mediterranean Sea (Fig. 1). The county has a population density of ca. 1100 hab·km<sup>-2</sup>, and is highly anthropized, with 15% agricultural and 30% urban land use (Rufí-Salís et al., 2019). The geomorphology of the area is structurally associated with the fracturing and sinking of blocks (NW-SE direction), which developed in a set of stream valleys (Catalan Water Agency, 2010). The geology of these valleys is dominated by Quaternary detrital sediments that constitute layers of gravels, sands, and clays, which result from chemical weathering and the dragging of granite materials through torrential courses. These Quaternary deposits constitute different aquifers corresponding with each stream valley (Fig. 1). Simultaneously, each stream valley forms an ephemeral stream. In Maresme County there are around 40 ephemeral streams, which represents a density of 1 ephemeral stream per kilometer of coastline. Annual precipitation in the area ranges from 350 to 930 mm y<sup>-1</sup> (2015 to 2020) and is mainly governed by EPE occurring in the autumn and spring seasons. Precipitation events with >75 mm d<sup>-1</sup> (corresponding to the 99<sup>th</sup> wet-day percentile) are here considered as EPE (Pendergrass and Knutti, 2018) and have a recurrence of ca. 13 months. In this area most of these streams are hydraulically disconnected from their alluvial aquifers and, therefore, surface runoff takes place only after the most significant rain events, with floods occurring in a period of hours after the EPE. The nature of tides in the Maresme region is semidiurnal, with an amplitude in the order of a few centimeters (~20 – 40 cm). The bathymetry of the Barcelona - Maresme continental shelf is dominated by steps and ridges, with moderate slopes (1.1°), and an average shelf width of 13 km (Durán et al., 2014).

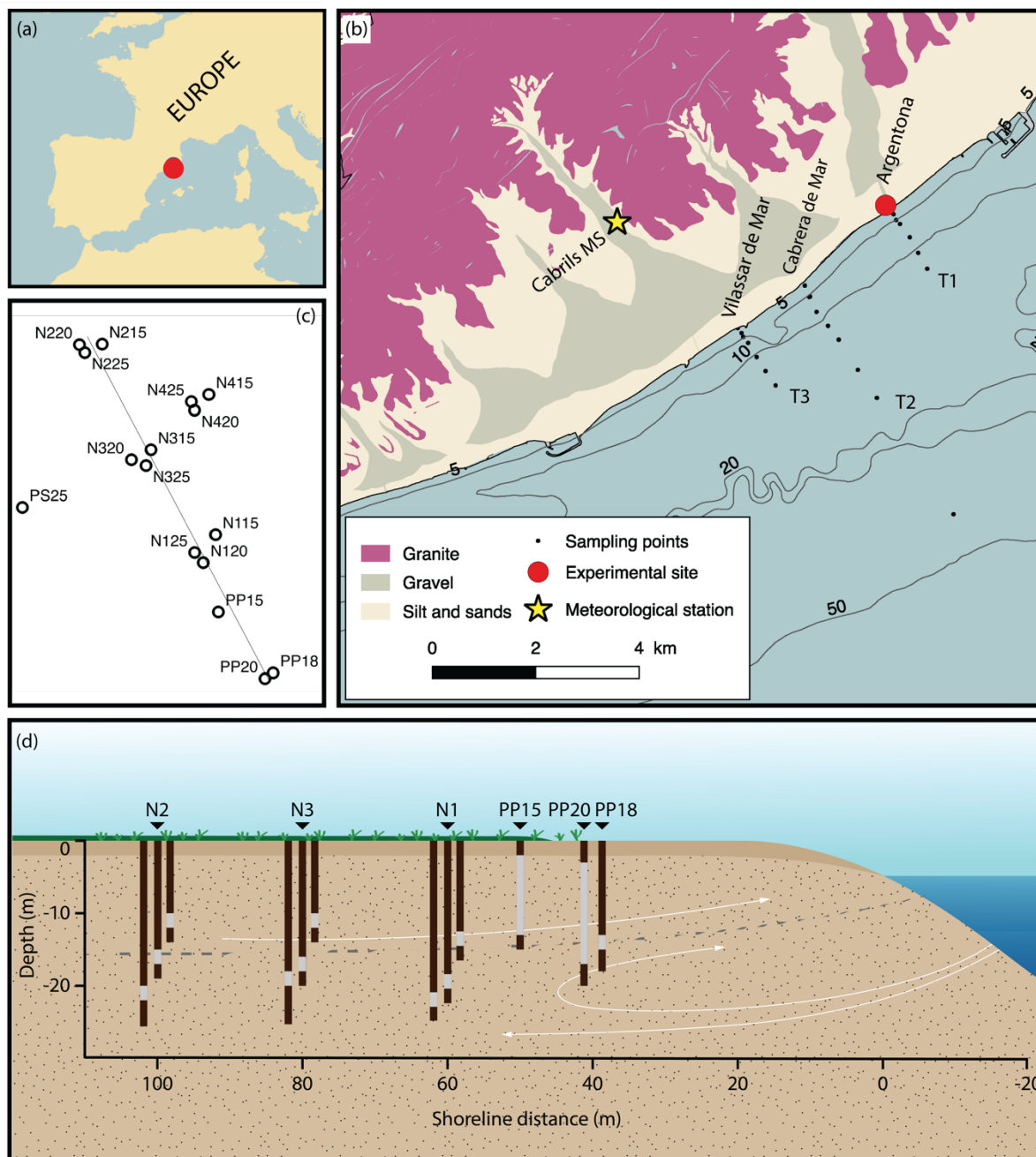


**Figure 1: Study site map. (a) Location map of Maresme County, (b) geological description, bathymetry, and sampling stations, (c) location map of the Medistraes site piezometers, and (d) schematic diagram of the piezometers and their screening sections within the perpendicular transect of the experimental site of Medistraes. T1, T2, and T3 are the offshore transects associated with the ephemeral streams of Argentona, Cabrera de Mar, and Vilassar de Mar, respectively.**



## 2.2 Field methods

Three samplings were conducted in the southern section of Maresme County during 2019 and 2020. The two first samplings  
85 (hereinafter P1 and P2, chronologically) were performed shortly after an EPE with an accumulated precipitation rate of ~90  
mm in one day. The EPE took place on October 22<sup>nd</sup> 2019 and P1 and P2 were conducted on October 25<sup>th</sup> and 29<sup>th</sup>, 2019 (~4  
and 8 days after the rainfall event, respectively). The third sampling (named BF, after “baseflow”) was conducted on March  
11<sup>th</sup> 2020, was not affected by any rainfall event, and was therefore considered to have been conducted under baseflow  
conditions (accumulated rainfall of 18 mm in the prior 40 days). Seawater samples were collected at different stations from  
90 three perpendicular transects to the coastline corresponding to the ephemeral streams of Argentona, Cabrera de Mar, and  
Vilassar de Mar (Transects T1, T2, and T3, respectively; Fig. 1). Each transect consisted of 7 offshore stations distributed  
along the first 1000 m. The central transect (T2) had three additional stations at 1500, 2000, and 4000 m from the coastline.  
Coastal seawaters were collected directly from the shore by filling 25 L water containers. At each station, surface and deep  
(only selected stations) seawater samples were collected by placing a submersible pump at ~0.5 m depth and ~1 m above the  
95 seabed, respectively.

Samples were collected for Ra isotopes ( $^{223}\text{Ra}$ ,  $^{224}\text{Ra}$ ,  $^{226}\text{Ra}$ , and  $^{228}\text{Ra}$ ; 25 – 120 L each sample), which are widely applied  
tracers of SGD (Garcia-Orellana et al., 2021) and nutrient analysis. Depth profiles of salinity and temperature were performed  
at each station by using a YSI 600XL probe. Groundwater samples for Ra isotopes (10 – 25 L) and nutrients were collected  
periodically from 2015 to 2020 in several piezometers at the experimental site of the Medistraes project, located in the coastal  
100 alluvial aquifer of the Argentona ephemeral stream (corresponding to Transect 1). The experimental site consists of 16  
piezometers located at 30 to 100 m from the coastline with screened depths of 15 to 25 m, with 2 m screened intervals for each  
(see Diego-Feliu et al., 2021; Folch et al., 2020; Palacios et al., 2019, for more details about the experimental site; Fig. 1).  
Each piezometer was purged with a submersible pump to remove at least three times the volume of stagnant water before  
sampling. Continuous in-situ groundwater level, conductivity, and temperature time-series were monitored at a shallow  
105 piezometric well (N3-15; 15 m depth, 2 m screened interval, from 11 to 13 m, 80 m from the coastline) using a CTD diver.  
Salinity and groundwater temperature, as well as seawater samples, were measured in-situ with two handheld probes (HANNA  
HI98192 and WTW COND 330I). Rainfall data was obtained from a meteorological station from the Meteorological Catalan  
Service (Servei Meteorològic de Catalunya; SMC) at the municipality of Cabrils (see Fig. 1).

## 2.3 Field methods

110 Samples collected for Ra isotopes both in seawater and groundwater were weighted and filtered through  $\text{MnO}_2$ -impregnated  
acrylic fibers, at a controlled flow rate ( $< 1 \text{ L min}^{-1}$ ) to ensure the quantitative adsorption of Ra onto the fibers (Moore and  
Reid, 1973). Fibers were then washed with Ra-free deionized water and partially dried to a fiber-water ratio of 1:1 (Sun and  
Torgersen, 1998). Each fiber was measured twice with the Radium Delayed Coincidence Counter (RaDeCC) (Moore and  
Arnold, 1996). Short-lived Ra isotopes ( $^{223}\text{Ra}$ ,  $T_{1/2} = 11.4 \text{ d}$ ;  $^{224}\text{Ra}$ ,  $T_{1/2} = 3.66 \text{ d}$ ) were quantified using the first RaDeCC



115 measurement. The activities of  $^{223}\text{Ra}$  are not reported in this study because the high  $^{224}\text{Ra}$  activities prevented the proper  
quantification of  $^{223}\text{Ra}$  with the RaDeCC system, due to cross-talk effect (Diego-Feliu et al., 2020). The second measurement,  
performed one month after sample collection, was used for quantifying the unsupported activity of  $^{224}\text{Ra}$  (excess  $^{224}\text{Ra}$ ;  $^{224}\text{Ra}_{\text{ex}}$ ),  
by accounting for the activity of its parent,  $^{228}\text{Th}$ , in the fiber. The quantification of  $^{224}\text{Ra}$  was made following the guidelines  
and limits proposed by Diego-Feliu et al. (2020) in order to avoid interferences inherent to the detection system, while  $^{224}\text{Ra}$   
120 uncertainties were estimated following Garcia-Solsona et al. (2008). The  $\text{MnO}_2$ -fibers were subsequently incinerated,  
grounded, and transferred to gamma counting vials. After radioactive equilibration ( $\sim 21$  d), the activities of long-lived Ra  
isotopes ( $^{226}\text{Ra}$ ,  $T_{1/2} = 1,600$  y;  $^{228}\text{Ra}$ ,  $T_{1/2} = 5.75$  y) were measured using a HPGe gamma spectrometer. The photopeaks of  
 $^{214}\text{Pb}$  (352 keV) and  $^{228}\text{Ac}$  (911 keV) were used to quantify the activities of  $^{226}\text{Ra}$  and  $^{228}\text{Ra}$ , respectively.  
Samples for the analysis of silicate ( $\text{SiO}_2$ ), phosphate ( $\text{PO}_4^{3-}$ ), nitrite ( $\text{NO}_2^-$ ), nitrate ( $\text{NO}_3^-$ ), and ammonia ( $\text{NH}_4^+$ ) were collected  
125 in 10 mL polyethylene vials after filtration through nylon syringe filters (pore size:  $0.45 \mu\text{m}$ ). Vials were immediately stored  
in a portable fridge and subsequently frozen at the laboratory until analysis. The analysis was performed using a colorimetric  
method with an Autoanalyzer AA3 HR (Seal Analytica). The detection limits of the method were 0.016, 0.020, 0.003, 0.006,  
and  $0.003 \mu\text{M}$  for  $\text{SiO}_4^{2-}$ ,  $\text{PO}_4^{3-}$ ,  $\text{NO}_2^-$ ,  $\text{NO}_3^-$ , and  $\text{NH}_4^+$ , respectively.

### 3 Results

#### 130 3.1 Meteorological and hydrological context

The temporal evolution of groundwater level, conductivity, significant wave height, mean sea level (MSL), and accumulated  
precipitation from October 2019 to April 2020 are shown in Fig. 2. Three major precipitation events occurred in October 2019  
( $\sim 90$  mm), December 2019 ( $\sim 100$  mm), and January 2020 ( $\sim 160$  mm), which had a direct impact on groundwater level and  
conductivity. These events are considered extreme precipitation events following the threshold value derived from the 99<sup>th</sup>  
135 wet-day percentile ( $\sim 75$  mm). After each EPE, the groundwater table from the shallow piezometer (N3-15) rose between 60  
and 130 cm, gradually recovering the previous values 7 to 10 days after the event. The magnitude in the increase of the  
groundwater level (60, 70, and 130 cm, respectively) correlated with the amount of accumulated rainfall corresponding to each  
EPE. Precipitation events were followed by a drastic reduction of groundwater conductivity at the shallow piezometer, reaching  
minimum values of  $\sim 1 \text{ mS cm}^{-1}$ , and a subsequent gradual increase before the next precipitation event (Fig. 2). As inferred by  
140 electric resistivity tomography profiles shown in Palacios et al. (2019), conductivity variations in the piezometric wells of the  
study site were not derived from dilution with low-conductivity rainwater, but associated with the movement of the mixing  
zone due to EPE. Significant wave height fluctuations occurred, associated mainly with changes in wind and atmospheric  
pressure during the EPEs, increasing rapidly from 2 to 5 m above the baseline value of approximately 0.5 m. Similarly, the  
MSL presented oscillations linked to the EPE, which are usually associated with atmospheric fronts and strong winds, and also  
145 to seasonal meteorology, with higher MSL values from October to December than from January to April.

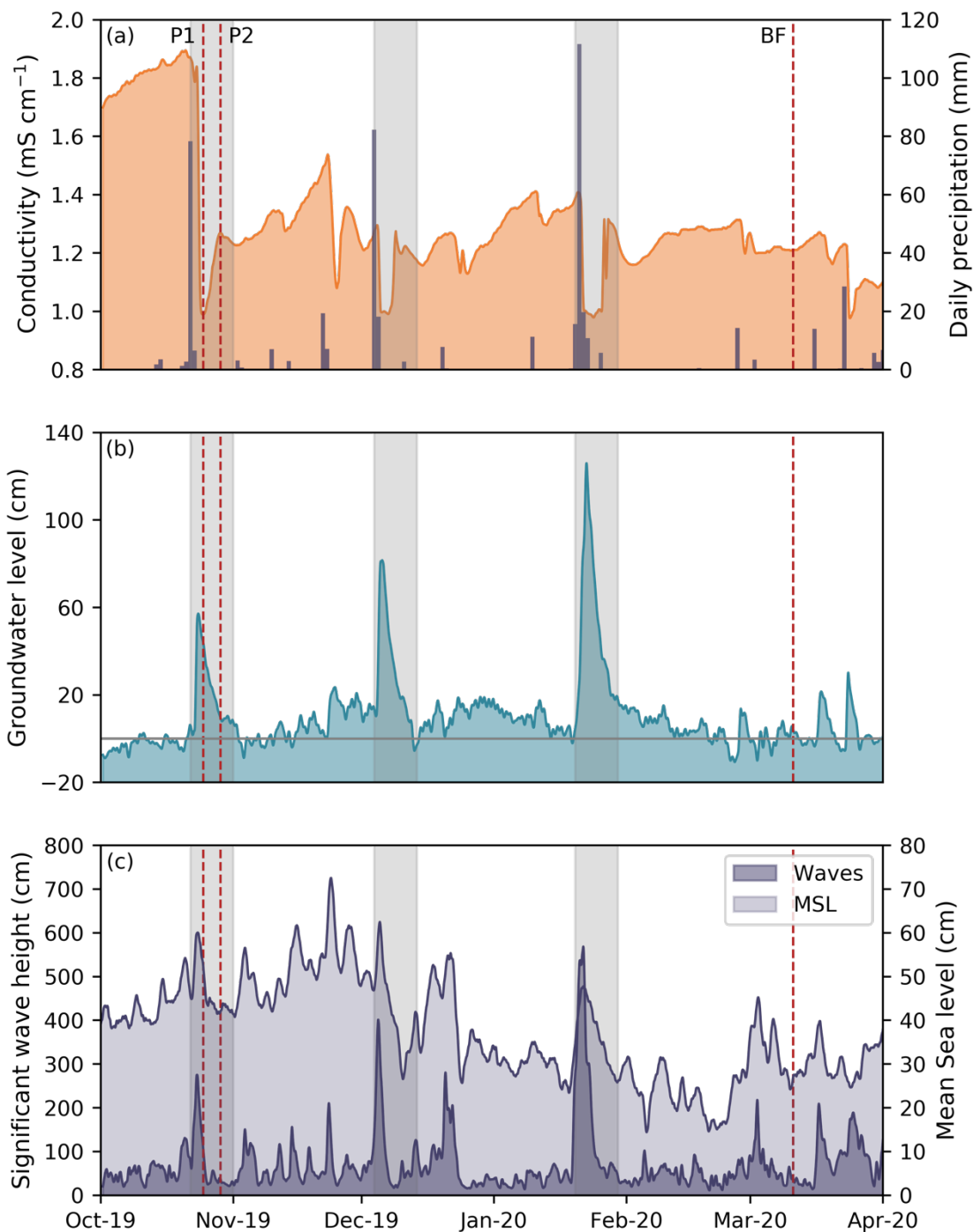


**Figure 2.** Temporal evolution of meteorological, oceanographical and hydrogeological data in Maresme County: (a) specific conductivity measured at the shallow piezometer N3-15 and accumulated precipitation (b) groundwater level, and (c) significant wave height and mean sea level. Groundwater level is displayed as the variation of



groundwater level relative to the values of March 2020. The data from the buoy and CTD-diver was smoothed by using a low-pass filter (12 h averaged). Red lines indicate the groundwater and seawater samplings performed at the study site (P1, P2, and BF) and grey bands indicate the EPEs that occurred during the monitoring period (10 days after the event are included in the band).

### 3.2 Radium and nutrient concentrations

The activities of Ra isotopes in groundwater samples measured during the 2015-2020 period in the Medistraes site ranged from 10 to 940, 10 to 550, and 1 to 50 Bq m<sup>-3</sup> for <sup>224</sup>Ra, <sup>228</sup>Ra, and <sup>226</sup>Ra, respectively (see supplementary information (SI); Fig. S1). The activities of Ra increased with groundwater salinity, presenting some variations that are mostly associated with differences in the geological matrix (Beck and Cochran, 2013; Webster et al., 1995). The seawater activities of <sup>224</sup>Ra and <sup>228</sup>Ra isotopes generally decreased with increasing distance offshore for all transects and seawater samplings (Fig. 3). Maximum activities were found in the first sampling after the rainfall event (P1) for <sup>224</sup>Ra (median: 14.4 Bq m<sup>-3</sup>, interquartile range (IQR): 11.7 – 19.9 Bq m<sup>-3</sup>) and <sup>228</sup>Ra (5.8 Bq m<sup>-3</sup>, IQR 4.9 – 7.1 Bq m<sup>-3</sup>). The seawater activities of <sup>224</sup>Ra and <sup>228</sup>Ra in subsequent samplings (P2 and BF) were three to five times lower than those of the sampling after the rainfall event (4.0 Bq m<sup>-3</sup>, IQR 2.4 – 10.2 Bq m<sup>-3</sup> for <sup>224</sup>Ra; and 1.4 Bq m<sup>-3</sup>, IQR 1.1 – 1.9 Bq m<sup>-3</sup> for <sup>228</sup>Ra). Seawater activities of <sup>226</sup>Ra were low, and comparable to open seawater activities in all samplings (1.8 Bq m<sup>-3</sup>, IQR 1.4 – 2.0 Bq m<sup>-3</sup>), revealing the lack of major inputs for this Ra isotope. Nutrient concentrations in groundwater from the experimental site of the Argentona ephemeral stream (2015-2020 period) ranged from 10 to 1070 μM for NO<sub>3</sub><sup>-</sup>, 0.1 to 3.9 μM for NO<sub>2</sub><sup>-</sup>, 0.3 to 40.1 μM for NH<sub>4</sub><sup>+</sup>, 0.8 to 10.1 μM for PO<sub>4</sub><sup>3-</sup>, and 50 to 230 μM for SiO<sub>4</sub><sup>2-</sup> (Fig. S2). Nitrate (NO<sub>3</sub><sup>-</sup>) and silica (SiO<sub>4</sub><sup>2-</sup>) presented a similar pattern, with maximum concentrations in low salinity samples (Sal < 10) and a downward trend with increasing groundwater salinity. Conversely, the concentrations of nitrite (NO<sub>2</sub><sup>-</sup>), phosphate (PO<sub>4</sub><sup>3-</sup>), and ammonia (NH<sub>4</sub><sup>+</sup>) were relatively low for most of the groundwater samples, except for those collected at the shallow piezometers for nitrite, intermediate for phosphate, and deep for ammonia (see SI; Fig. S2).



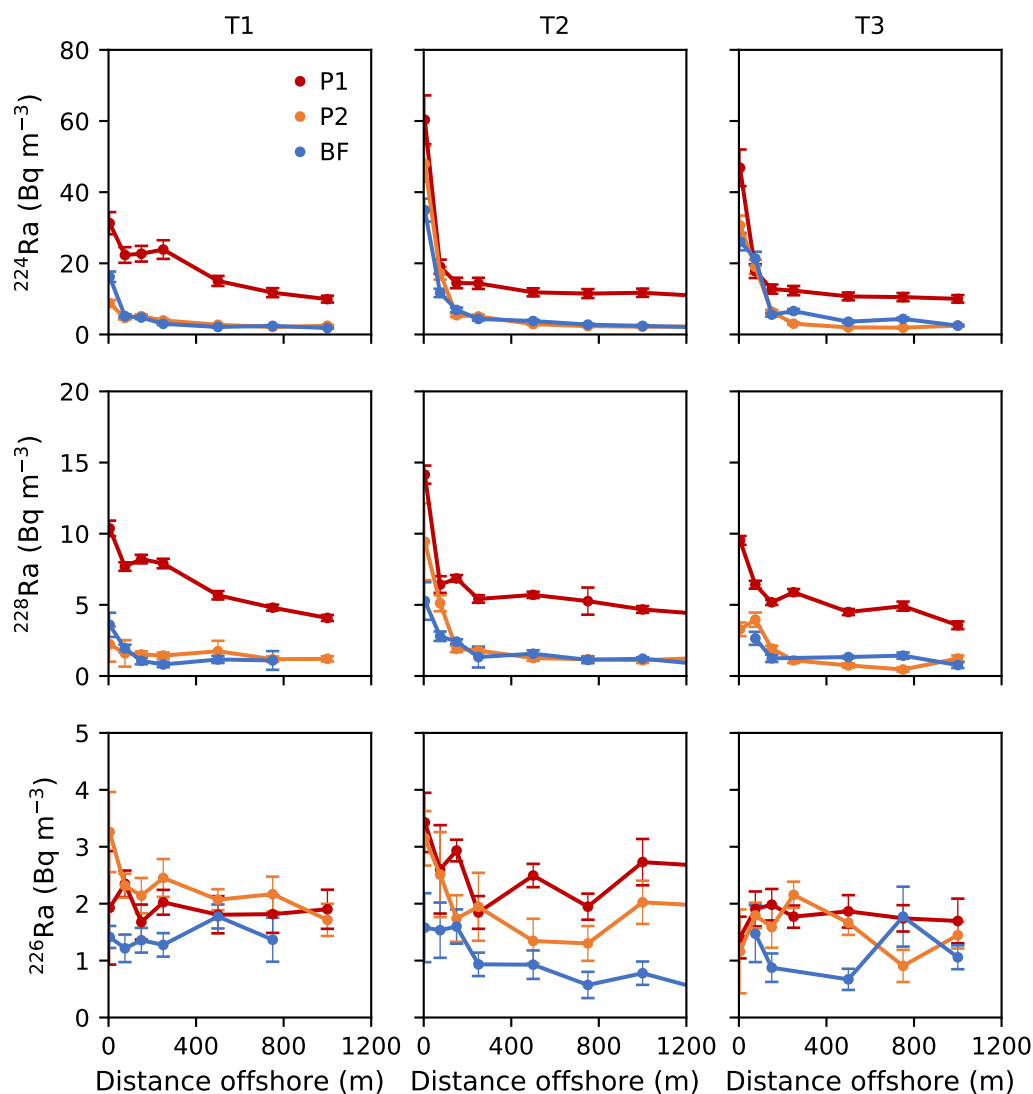


**Figure 3.** Radium isotopes activities ( $^{224}\text{Ra}$ ,  $^{228}\text{Ra}$ , and  $^{226}\text{Ra}$ ) in coastal seawater samples collected during the samplings performed in October 2019 (P1 and P2) and March 2020 (BF) for the three transects perpendicular to the coastline corresponding to the ephemeral streams of Argentona (T1), Cabrera de Mar (T2), and Vilassar de Mar (T3).

## 4 Discussion

### 4.1 Groundwater and nutrient fluxes calculation



#### 4.1.1 Pathways of submarine groundwater discharge

Submarine Groundwater Discharge incorporates a set of water flow processes involving the discharge of fresh groundwater and the circulation of seawater through permeable sediments (Garcia-Orellana et al., 2021; Michael et al., 2011; Santos et al., 2012). The driving forces and pathways of these processes likely determine the extent of the chemical reactions occurring in the subterranean estuary (Moore, 1999). Therefore, considering all the different SGD pathways concurrently occurring in a specific study site is fundamental for deriving reliable estimates of SGD and associated nutrient fluxes (Garcia-Orellana et al., 2021). Here, we define terrestrial groundwater discharge as the combined discharge of meteoric groundwater and density-driven circulated seawater, and marine groundwater discharge as those processes solely involving the circulation of seawater through permeable sediments (i.e., beach-face circulation, porewater exchange).

Radium isotopes represent one of the most common techniques for quantifying the fluxes of groundwater and associated nutrients to the coastal ocean (Garcia-Orellana et al., 2021; Taniguchi et al., 2019). These isotopes can additionally be instrumental for differentiating SGD pathways, since their enrichment rates strongly depend on the transit time of groundwater through the coastal aquifer (e.g., Diego-Feliu et al., 2021; Michael et al., 2011). Coastal seawater samples collected during the three samplings performed in Maresme County were enriched in both  $^{224}\text{Ra}$  and  $^{228}\text{Ra}$  relative to offshore waters (Fig. 3), suggesting the occurrence of a land-based Ra source. Whilst the enrichment in  $^{224}\text{Ra}$  may result from any groundwater discharge, regardless of spatiotemporal scale, due to its short half-life ( $^{224}\text{Ra}$  is enriched in all SGD pathways), coastal waters enriched in  $^{228}\text{Ra}$  may be indicative of long-scale SGD pathways (e.g., terrestrial groundwater discharge; Rodellas et al., 2017; Tamborski et al., 2017a).

The activity ratio (AR) of  $^{224}\text{Ra}/^{228}\text{Ra}$  can similarly be used to evaluate the temporal scale of SGD pathways (Diego-Feliu et al., 2021). Thus, the  $^{224}\text{Ra}/^{228}\text{Ra}$  AR found in coastal seawater samples after the EPE from October 2019 decreased from a baseline value of 6 to approximately 4. This decrease is simultaneously followed by an increase in absolute  $^{228}\text{Ra}$  activities, which are two-times higher than those in baseflow conditions (Fig. 3). Both trends may indicate that the relative contribution of the terrestrial component of SGD, which is characterized by  $^{224}\text{Ra}/^{228}\text{Ra}$  ARs close to the equilibrium value (1.0 to 2.2; Diego-Feliu et al., 2021), increased during the occurrence of the EPE. Thus, based on the application of Ra isotopes and the  $^{224}\text{Ra}/^{228}\text{Ra}$  activity ratio, the discharge of terrestrial and marine groundwater occurs concurrently at the study site.

#### 4.1.2 Submarine groundwater discharge

Submarine groundwater discharge associated with terrestrial and marine water flows were determined by means of a steady-state mass balance of  $^{224}\text{Ra}$  and  $^{228}\text{Ra}$ . The assumptions, considerations, and models used to estimate SGD are discussed in detail in appendix A. The sampling influenced by the EPE of October 2019 (P1) presented the highest total SGD (terrestrial and marine) ( $510 \cdot 10^3 \text{ m}^3 \text{ km}^{-1} \text{ d}^{-1}$ , IQR:  $320 - 890 \cdot 10^3 \text{ m}^3 \text{ km}^{-1} \text{ d}^{-1}$ ), one order of magnitude higher than those flows from subsequent samplings:  $40 \cdot 10^3 \text{ m}^3 \text{ km}^{-1} \text{ d}^{-1}$  (IQR:  $30 - 90 \cdot 10^3 \text{ m}^3 \text{ km}^{-1} \text{ d}^{-1}$ ) for P2 and  $70 \cdot 10^3 \text{ m}^3 \text{ km}^{-1} \text{ d}^{-1}$  (IQR:  $40 - 110 \cdot 10^3 \text{ m}^3 \text{ km}^{-1} \text{ d}^{-1}$ ) for BF (Fig. 4). Thus, the effect of this EPE on the discharge of groundwater lasts only for a few days, as the SGD



estimates of the second sampling (P2; 8 days after the event) are comparable to those from baseflow conditions. Besides the similitudes in SGD estimates from these two samplings (P2 and BF), they also present similar groundwater levels, conductivities, and Darcy's flow estimates (Fig. 2 and Fig. B1). Thus, the temporal extent of the EPE effects on SGD is consistent with the recovery of groundwater level, which commonly occurs from 7 to 10 days after the rainfall ceases (Fig. 2). In baseflow conditions, the terrestrial component of SGD (including fresh and brackish density-driven discharge) represented 60% of the total SGD (Fig. 4). The relative contribution of this SGD component increased after the rainfall event of October 2019 to up to 75% of the total SGD. This is consistent with the variation on the  $^{224}\text{Ra}/^{228}\text{Ra}$  AR in coastal seawater after the EPE (see Section 4.1.1) and coherent with Darcy's flow calculations (Appendix B). These estimates of the relative contribution of the terrestrial component are generally much larger than previous estimates for the Mediterranean Sea (1 - 25%, Rodellas et al., 2015), global estimates (10%, Kwon et al., 2014; 0.06%, Luijendijk et al., 2020), and local studies (5 - 55%; Alorda-Kleinglass et al., 2019; Beck et al., 2008; Kiro et al., 2014; Knee et al., 2016; Rodellas et al., 2017; Tamborski et al., 2017a). This difference most likely emphasizes the role of alluvial aquifers in ephemeral streams-dominated areas as a preferential pathway of terrestrial groundwater discharge (Jou-Claus et al., 2021). It should be noted however that any comparison between studies should be considered as semi-quantitative, firstly because the diverse geological settings where SGD studies are conducted result in diverse SGD pathways and implications, and secondly because different studies use disparate methods that can capture different components of SGD depending on their spatial and temporal scales (Taniguchi et al., 2019).

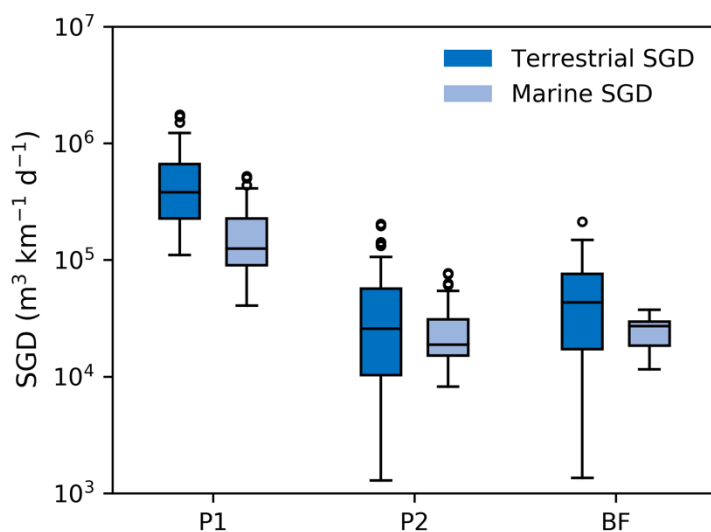


**Figure 4.** Coastal-normalized flow of terrestrial and marine submarine groundwater discharge (dark and light blue, respectively) for the three samplings at Maresme County.



#### 4.1.3 SGD-driven nutrient fluxes

215 SGD-driven nutrient fluxes were estimated by considering the Ra-derived flows of terrestrial and marine SGD and the  
respective nutrient concentration in groundwater from both fractions (see Appendix A). Total SGD-driven fluxes in baseflow  
conditions for dissolved inorganic nitrogen (DIN), dissolved inorganic phosphorus (DIP), and dissolved silicate (DSi) derived  
from median SGD estimates in the study site were 16.2, 0.06, and  $5.4 \cdot 10^3$  mol km<sup>-1</sup> d<sup>-1</sup>, respectively (Fig. 5). The median  
fluxes, normalized by the study site area, were lower compared with median SGD-derived nutrient fluxes estimated worldwide  
220 for DIP and DSi, but significantly higher for DIN (2.7 times higher; Santos et al., 2021). The DIN:DIP ratio was 390:1, much  
higher than the Redfield ratio of 16:1, but comparable with SGD-derived input in the Mediterranean Sea (80:1–430:1; Rodellas  
et al., 2015) and in studies worldwide ( $259 \pm 1090:1$ ; Santos et al., 2021). The high loads of N and the disproportionate ratio  
DIN:DIP relative to the Redfield ratio in the study site may result from the lixiviation of nitrogen from agricultural activities  
(representing ~15% of the total land-use; Rufi-Salís et al., 2019), and the attenuation of P along groundwater flow paths due  
225 to adsorption onto Mn/Fe oxides present in the coastal aquifer (Robinson et al., 2018; Spiteri et al., 2007, 2008b).  
After an EPE, the supply of all nutrients increased due to the higher terrestrial and marine SGD associated with these episodes  
(Fig. 5). Fluxes after the EPE (P1) were 9 times higher for DIN and 7 times higher for DIP and DSi than those in baseflow  
conditions. The predominant pathway for DIN, DIP, and DSi discharge to the coastal ocean was the terrestrial component of  
SGD. This pathway represented ~60% of the total inputs of DIP and DSi in baseflow conditions and up to ~75% after an EPE  
230 (Fig. 5). Nitrogen inputs during EPE and in baseflow conditions were chiefly governed by the discharge of terrestrial SGD  
(~99% of the total DIN inputs; Fig. 5). The significant difference between the supply of nitrogen through terrestrial and marine  
SGD relies on the high concentrations of nitrate (~1,000 µM) in coastal aquifer freshwater (see SI; Fig. S2), which exceed the  
maximum groundwater concentration for drinking water set by the World Health Organization (WHO, 2011). Contrastingly,  
marine SGD is a relevant source of nitrite and ammonia, representing ~70% and ~40% of the total fluxes, respectively. It  
235 should be noticed that nutrient fluxes were estimated by multiplying the volumetric water flux of terrestrial and marine SGD  
by the minimum nutrient concentration from a set of onshore samples, selected following the criteria used for the Ra  
endmembers, as explained in the appendices (see appendix A.2.4). Since it was not possible to directly collect the discharging  
groundwater, by using onshore samples we are implicitly assuming that no nutrient transformation occurred between the  
sampling point and the discharge point, within the subterranean estuary (Cook et al., 2018). It should also be noted that these  
240 SGD-derived nutrient estimates may be biased due to the groundwater endmember selection, since nutrient concentrations in  
discharging groundwaters may vary during EPE due to dilution, increasing lixiviation of fertilizers, or enhancement of  
biogeochemical reactions in the mixing zone of coastal aquifers (Spiteri et al., 2008a).

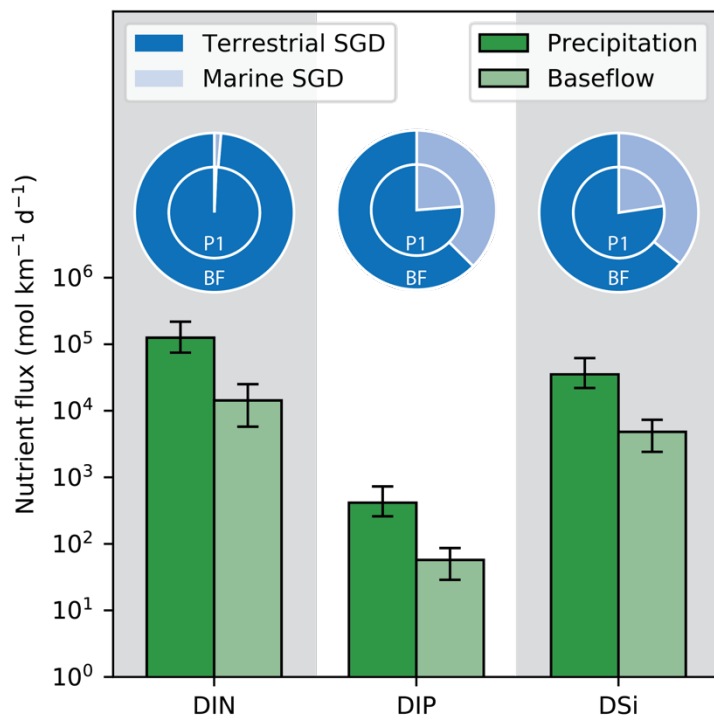


**Figure 5. Median SGD-derived nutrient fluxes of dissolved inorganic nitrogen, dissolved inorganic phosphorus, and dissolved silicate at Maresme County during the EPE of October 2019 (P1) and in baseflow conditions (BF) (fluxes normalized by the coastline length). Error bars indicate the interquartile range (25% and 75% percentile). Inner and outer pie charts indicate the relative contribution of terrestrial (dark blue) and marine (light blue) SGD during EPE and in baseflow conditions, respectively.**

## 4.2 Implications of EPE on SGD and associated nutrient fluxes

### 4.2.1 Episodic events

245 Although several studies have focused on understanding the seasonal dynamics of SGD (Charette, 2007; Gwak et al., 2014; Michael et al., 2005; Rodellas et al., 2017), limited research has been done on SGD driven by episodic events (Adyasari et al., 2021; Wilson et al., 2011). This is mainly because of the inherent difficulties related to monitoring and sampling during and after these extreme events. Some studies have already shown that SGD may vary in direct or delayed response to meteorological and oceanic episodic events such as sea-level anomalies (Gonneea et al., 2013), waves (Bakhtyar et al., 2012; Rodellas et al., 2020; Sawyer et al., 2013), hurricanes (Hu et al., 2006), typhoons (Cho et al., 2021; Sugimoto et al., 2016), and temperature inversion (Moore and Wilson, 2005). Regarding SGD induced by precipitation events: Sugimoto et al. (2016) reported high values of SGD eleven days after a precipitation event in Obama Bay (Japan); Gwak et al. (2014) suggested that SGD in the II-Gwang watershed (South Korea) was partially triggered by intensive precipitation events; and Uddameri et al. (2014) indicated that precipitation events associated with the Emili hurricane contributed to the SGD in Baffin Bay (USA). At



255 our study site, the significant increase (1 order of magnitude; Fig. 4) in both the terrestrial and marine SGD after EPE, may be  
mediated by different processes: (1) increase of terrestrial groundwater discharge due to aquifer infiltration of rainfall,  
subsequent increase of hydraulic gradient, and displacement of stored water towards the sea (Anwar et al., 2014; Palacios et  
al., 2019; Santos et al., 2012; Yu et al., 2017), (2) increase in the exchange of seawater and density-driven discharge due to  
movements of the fresh-saltwater mixing zone, and (3) increase of shoreface circulation of seawater and porewater exchange  
260 due to the effect of sea level rise and waves associated with the EPE (Fig. 2).

The higher total SGD driven by EPE, especially the increase of terrestrial relative to marine SGD during these episodic events  
(Fig. 4), induces the transport of large amounts of nutrients from the freshwater fraction of coastal aquifers into the coastal  
ocean. These fluxes, which are substantially higher than those in baseflow conditions (Fig. 5), may represent a significant  
periodic and episode-related nutrient input of particular relevance in sites where surface water renewal is limited (e.g., coastal  
265 lagoons and/or semi-enclosed bays), EPE occurs frequently (e.g., Mediterranean region), and the response to EPE is fast due  
to the geological and geomorphological characteristics of the coastline (e.g., alluvial aquifers in ephemeral stream-dominated  
areas, such as Maresme County). However, in other areas the response to EPEs may be much slower. For instance; aquifers  
with a high thickness of vadose zones, confined aquifers with recharge areas far from the coastal zones, or systems with soils  
with water deficits (among other factors), may smooth or delay the effects of EPE. The biological and ecological implications  
270 of these events- which may include eutrophication, formation of red and green tides, and mass fish death (Hu et al., 2006; Lee  
et al., 2010; Montiel et al., 2019; Valiela et al., 1990; Zhao et al., 2021)- are far from being understood, and require further  
attention.

#### 4.2.2 Annual SGD estimates

A proper understanding of the temporal patterns of SGD in local to regional-scale studies is essential for deriving annual  
275 estimates for predicting reliable ocean budgets of nutrients and other dissolved compounds (Luijendijk et al., 2020; Santos et  
al., 2021). However, most SGD studies are conducted in periods with stable meteorological conditions to evaluate baseflow  
SGD and associated nutrient, metal, or contaminant fluxes. Based on the results obtained from monitoring the EPE occurred  
at Maresme County in October 2019, the discharge of groundwater associated to this single event accounted for 13% (IQR: 5  
– 40%) and 8% (IQR: 5 – 18%) of the annual terrestrial and marine fraction of SGD, respectively. Moreover, the nutrient  
280 inputs resulting from this event (lasting only 8 days; ~2% of the year) represented 13% (IQR: 5 – 40%) for DIN, and 11%  
(IQR: 5 – 30) for DIP and DSi, of the yearly supply of nutrients at the study site. The increase in SGD-driven nutrient fluxes  
during these events may be mediated, on the one hand by the total SGD increase, but also because this increase is more  
significant for terrestrial SGD, which presents higher concentrations of nutrients (see supplementary information; Fig. S2),  
relative to marine SGD. These results suggest that annual estimates based on samplings conducted in baseflow conditions may  
285 systematically underestimate SGD and associated nutrients, particularly at study sites affected by EPEs or other episodic events  
that can significantly impact SGD. Periodic and seasonal samplings may be taken as snapshots, and only representative of the  
time periods with similar environmental conditions. A better characterization of the hydrological and meteorological context



is necessary in pursuit of more reliable annual estimates, which may include seasonal and episodic-related variations. In this scenario, alternative methods such as groundwater level monitoring, Darcy's law calculations, electric resistivity tomography  
290 characterization, among other methods, may be instrumental in the design of proper sampling strategies and to capture seasonal and episodic variations (e.g., Folch et al., 2020; Palacios et al., 2019).

#### 4.2.3 Climate change

Climate change and its associated social and environmental impacts have become one of the most pressing scientific challenges for the 21<sup>st</sup> century. This requires the acquisition of a holistic and integrative knowledge of systems and processes for modelling  
295 and predicting future scenarios. Fundamental research relating environmental key variables (e.g., temperature, sea-level rise, precipitation) with social processes (e.g., land demand, coastal overpopulation, groundwater squeeze) becomes crucial to this aim. Research on SGD is no exception to this trend and, in recent decades, several studies have evaluated the key factors contributing to groundwater flows discharging into the ocean. Some examples of SGD research linked to climate change include; understanding sea-level and/or tidal controls on SGD (Gonneea et al., 2013; Wilson et al., 2015); the influence of  
300 land-use changes (Rufi-Salís et al., 2019); the relationship to increasing seawater intrusion (Werner et al., 2013); and the fate and evolution of nutrients in groundwater (Beusen et al., 2013; Van Meter et al., 2018; Tait et al., 2014).

The precipitation-recharge relationship is one of the key parameters influencing the discharge of groundwater. Indeed, the amount of precipitation and the frequency and/or distribution of rainfall events, together with the hydrogeological characteristics of the receiving aquifers, strongly affects both the quantity and chemical quality of terrestrial groundwater  
305 discharge to the ocean (Kundzewicz and Döll, 2009; Stigter et al., 2014). Climate models indicate substantial spatial variation in future changes to average precipitation. Whilst the increased specific humidity and transport of water vapor from tropic regions is likely to increase the amount of precipitation in high latitude land masses, precipitation in subtropical and semi-arid regions, like the Mediterranean Sea, is expected to decrease. Simultaneously, EPE in these regions are likely to increase in intensity and frequency (IPCC, 2021). Consequently, the yearly recharge of groundwater associated with precipitation in the  
310 Mediterranean region may diminish, also reducing the annual discharge of groundwater. In that scenario, EPEs may become a major driving force of SGD, having a dominant significance in the annual fluxes of solutes to the coastal ocean.

The potential relevance of EPEs on SGD in future conditions can be qualitatively evaluated for Maresme County by considering the period from October 2019 to April 2020, when 3 precipitation events of >75 mm occurred (Fig. 2). Since the historical recurrence of EPE in the area is around 13 months (based on the meteorological data from 2015 to 2020), this 7-  
315 month period can be considered as a future-like year with increased recurrence of EPE. Assuming that each one of the EPE produces an increase in SGD comparable to the event monitored in this study, the relative contribution of SGD during EPEs would represent 30% (IQR: 15 – 70%) and 22% (15 – 40%) of the annual SGD issued by the terrestrial and marine fraction, respectively. Similarly, nutrient fluxes associated with EPE for this period would represent 34% (IQR: 15 – 70%) for DIN and 30% (IQR: 15 – 60%) for DIP and DS<sub>i</sub> of the yearly nutrient inputs supplied by SGD. Notice that due to the assumptions made  
320 in the determination of groundwater and nutrient fluxes (e.g., steady state, endmember selection; see appendix A), the estimates



are seemingly conservative, especially considering that the monitored EPE is minor relative to other EPEs occurring in 2019 and 2020 (Fig. 2). These estimates emphasize the need for integrating episodic events, such as EPE, in future climate change scenarios, in order to properly constrain the fluxes of groundwater and solutes to the coastal ocean driven by SGD.

## 5 Conclusions

325 Extreme precipitation events are potential drivers of submarine groundwater discharge and driven nutrients to the coastal  
ocean. The lack of studies assessing the impact of these episodic events mask the implications that they may have for coastal  
geochemical cycles, coastal ecosystems, nutrient budgets, and hydrological cycle estimates. We have assessed the fluxes of  
SGD induced by an EPE in an ephemeral stream-dominated basin of the western Mediterranean Sea. SGD induced by the EPE  
increased by one order of magnitude and represented up to 13 and 8% of the total annual discharge of groundwater of terrestrial  
330 and marine SGD, respectively. Similarly, fluxes of nutrients driven by SGD during an EPE represented 11 - 13% of the annual  
total SGD, and up to ~30% during abnormally rainy seasons. This study highlights the relevance of these extreme events on  
the discharge of groundwater and solutes to the coastal ocean, noting their implications for annual SGD estimates and the  
possible consequences on coastal biogeochemistry cycles. The results of this study contribute to the understanding of the  
evolution of SGD with respect to future climate change scenarios, presenting an opportunity for streamlining future research  
335 in order to help managers and policy makers better estimate SGD and its related consequences.

## 6 Appendices

### A SGD and nutrient fluxes calculations

In this appendix, we develop the methodology used for determining the SGD and associated nutrient fluxes to the coastal  
ocean. This includes the definition of the conceptual model and the discussion of the model assumptions used in the  
340 calculations.

#### A.1 Radium mass balance

The magnitude of SGD and its associated nutrient fluxes are quantified in this study by using Ra isotopes, which is one of the  
most commonly applied techniques (Garcia-Orellana et al., 2021; Taniguchi et al., 2019). Whilst single isotopes can be used  
for quantifying SGD driven by single pathways, the combination of different isotopes is instrumental in discriminating SGD  
345 in sites with multiple pathways (Alorda-Kleinglass et al., 2019; Charette, 2007; Rodellas et al., 2017; Tamborski et al., 2017b).  
In this study, Ra isotopes are used for discriminating and quantifying both the fluxes of terrestrial and marine SGD. Whilst  
terrestrial SGD represents a net input of water to the ocean, marine SGD comprises disparate discharge processes solely  
involving the circulation of seawater through permeable sediments or the coastal aquifer (i.e., porewater exchange, shoreface





circulation of seawater, seasonal exchange of seawater; Garcia-Orellana et al., 2021; Michael et al., 2011). A steady-state mass  
 350 balance of short-lived  $^{224}\text{Ra}$  ( $T_{1/2} = 3.66$  d) and long-lived  $^{228}\text{Ra}$  ( $T_{1/2} = 5.75$  y) isotopes was constructed as follows:

$$F_{TSGD} \cdot {}^{228}\text{Ra}_{TSGD} + F_{MSGD} \cdot {}^{228}\text{Ra}_{MSGD} = \frac{I_{ex-Ra228}}{T_F} + I_{Ra228} \cdot \lambda_{Ra228}$$

$$F_{TSGD} \cdot {}^{224}\text{Ra}_{TSGD} + F_{MSGD} \cdot {}^{224}\text{Ra}_{MSGD} = \frac{I_{ex-Ra224}}{T_F} + I_{Ra224} \cdot \lambda_{Ra224}$$
(A1)

The two terms on the right-hand side of Eq. (A1) represent the Ra outputs and include the offshore exchange of Ra, due to the  
 mixing between coastal and open ocean waters, and Ra decay. The terms  $I$  and  $I_{ex}$  refer to the mean inventories [ $\text{Bq m}^{-1}$ ] of  
 Ra and excess Ra (inventory of excess Ra concentrations in coastal waters relative to open ocean), respectively,  $T_F$  is the Ra  
 355 flushing time [d], and  $\lambda$  is the Ra decay constant [ $\text{d}^{-1}$ ]. The mean Ra inventories were determined by averaging the activity (or  
 excess activity) [ $\text{Bq m}^{-3}$ ] of Ra at each station normalized by depth and distance to the shore. The normalization was made by  
 integrating the rectangular trapezoid area confined within the distance between two subsequent stations and their respective  
 depth. The two terms on the right-hand-side of Eq. (A1) account for Ra inputs to the study site, which are supplied via terrestrial  
 (combined discharge of meteoric groundwater and density-driven circulated seawater) and marine (processes solely involving  
 360 the circulation of seawater through permeable sediments; beach-face circulation, porewater exchange) SGD [ $F_{Ra}$ ;  $\text{Bq m}^{-1} \text{d}^{-1}$ ].  
 The activities [ $\text{Bq m}^{-3}$ ] of Ra in the discharging groundwater ( $Ra_{TSGD}$  and  $Ra_{MSGD}$ ; Ra endmember) were used to convert the  
 Ra flux of both isotopes concurrently, to a coastline-normalized volumetric flow [ $\text{m}^3 \text{km}^{-1} \text{d}^{-1}$ ] for each of the SGD pathways  
 (Terrestrial SGD,  $F_{TSGD}$  and Marine SGD,  $F_{MSGD}$ ). The terms and values used for the Ra mass balance for each sampling are  
 shown in Table A1.

**Table A1. Definition of terms, values and units used for the Ra mass balance for each sampling (P1, P2 and BF).  
 Data in brackets represent the interquartile range (1st and 3rd quartile).**

Term	Definition	Values			Units
		P1	P2	BF	
$I_{Ra224}$	$^{224}\text{Ra}$ inventory	113±15	26±2	31±9	$\cdot 10^3 \text{ Bq} \cdot \text{m}^{-1}$
$I_{ex-Ra224}$	$^{224}\text{Ra}$ excess inventory	98±15	23±2	28±9	$\cdot 10^3 \text{ Bq} \cdot \text{m}^{-1}$
$I_{Ra228}$	$^{228}\text{Ra}$ inventory	46±3	11±2	9±3	$\cdot 10^3 \text{ Bq} \cdot \text{m}^{-1}$
$I_{ex-Ra228}$	$^{228}\text{Ra}$ excess inventory	41±3	10±2	8±3	$\cdot 10^3 \text{ Bq} \cdot \text{m}^{-1}$
$F_{Ra-224}^{*1}$	$^{224}\text{Ra}$ flux	62±9	9±1	11±4	$\cdot 10^3 \text{ Bq} \cdot \text{m}^{-1} \cdot \text{d}^{-1}$
$F_{Ra-228}^{*1}$	$^{228}\text{Ra}$ flux	16.8±1.3	1.8±0.4	1.6±0.5	$\cdot 10^3 \text{ Bq} \cdot \text{m}^{-1} \cdot \text{d}^{-1}$
$F_{Ra-224}/F_{Ra-228}$	$^{224}\text{Ra}/^{228}\text{Ra}$ flux ratio	3.7±0.3	5.2±1.2	7.6±2.7	-



$T_F^{*2}$	Ra flushing time	2.4±0.9	5.6±1.9	5.0±1.7	d
<b>Unknowns</b>					
$F_{FSGD}$	Fresh SGD flow	380 (235 - 660)	25 (10 - 55)	45 (15 - 75)	$\cdot 10^3 \text{ m}^3 \cdot \text{km}^{-1} \cdot \text{d}^{-1}$
$F_{RSGD}$	Recirculated SGD flow	125 (90 - 225)	20 (15 - 30)	25 (20 - 30)	$\cdot 10^3 \text{ m}^3 \cdot \text{km}^{-1} \cdot \text{d}^{-1}$

\*1 Flux of Ra supplied by terrestrial and marine SGD, left-hand side of Eq. (A1)

\*2 Radium fluxing time determined as water apparent age following Moore (2000)

## 365 A.2 Model assumptions and considerations

### A.2.1 Sources and sinks of Ra

The proposed model for quantifying the Ra flux to the sea assumes that terrestrial and marine groundwater discharge are the only sources of Ra at the study site (Eq. A1). Diffusive fluxes of Ra from sediments were considered negligible, due to the presence of coarse-grained sands with low specific surface area (Luek and Beck, 2014) and are assumed to represent low (10%) inputs compared to the total Ra inputs (Beck et al., 2007; Garcia-Orellana et al., 2014, 2021). Ra inputs from surface water were also discarded for the sampling conducted in March 2020 (BF) due to the total absence of runoff during the sampling period. In October 2019, 4 days before the first sampling conducted at the study site, runoff occurred in direct response to an EPE (~90 mm). However, considering the flushing time of Ra isotopes in the coastal system (see S1.2.2), the Ra delivered by this punctual runoff may have decreased by >90% for the first sampling (P1) and by >99% for the second sampling (P2), due to decay and mixing with offshore waters. It is thus assumed that runoff for these samplings represents a minor source of Ra at the study site relative to that from SGD. Atmospheric deposition was discarded as a major source of Ra since its contribution in small-scale study sites is often <<1% (Garcia-Orellana et al., 2021). Production of Ra from dissolved Th was implicitly included by reporting the activities of Ra isotopes as ‘excess’ Ra activities (activities non-supported by their progenitors). The decay of Ra and the exchange with offshore waters were considered as the major sinks of Ra. The decay was assessed via the Ra inventories at in the study site and the offshore exchange, by evaluating the flushing time of Ra ( $T_F$ ).

### A.2.2 Radium flushing time

The flushing time of Ra ( $T_F$ ) is a parameter that describes the transport of Ra in surface water bodies due to advection and dispersion processes (Monsen et al., 2002). In Ra mass balances, this parameter is fundamental for evaluating the exchange of Ra between coastal and offshore waters. In this work, rather than evaluating Ra flushing times, we used  $^{224}\text{Ra}/^{228}\text{Ra}$  of coastal and offshore waters (1,000 m from coastline) to determine the water apparent age ( $T_W$ ) (Moore, 2000). The water apparent age is a good proxy for temporal scales of advective and mixing processes occurring at the study site. Coastal waters in Maresme County presented  $^{224}\text{Ra}/^{228}\text{Ra}$  activity ratios ranging from 1.6 to 2.9 times higher than those of offshore waters, which led to seawater apparent ages of  $2.4 \pm 0.9$ ,  $5.6 \pm 1.9$ , and  $5.0 \pm 1.7$  days for the first, second, and third sampling, respectively. The lower



390 seawater residence time of the first sampling is coherent with the oceanographic conditions (e.g., higher winds, waves and  
currents that enhanced advection and exchange with offshore waters) linked to the extreme precipitation event occurring 4  
days before (see Fig. 2).

### A.2.3 Steady state conditions

Steady state conditions (i.e., tracer inventories do not vary with time;  $da/(dt \cdot V) = 0$ ) are often assumed in Ra mass balances  
(e.g., Alorda-Kleinglass et al., 2019; Beck et al., 2008; Rodellas et al., 2017). This assumption implies that Ra inputs and  
395 outputs are balanced for a time period equivalent to the tracer residence time in the system (Rodellas et al., 2021). In Maresme  
County, the tracer residence time ranged from 1.6 to 2.6 days for  $^{224}\text{Ra}$  and from 2.4 to 5.6 days for  $^{228}\text{Ra}$ . The tracer residence  
time can be estimated by dividing the radium inventory in surface waters by the sum of all losses (i.e., radioactive decay and  
exchange with offshore waters) (Rodellas et al., 2021). The assumption of steady state may therefore not be valid due to the  
significant difference between Ra activities from the first and second samplings (P1 and P2; Fig. 3), which were carried out  
400 only 4 days apart. However, assuming steady state conditions instead of a continuous decrease of activities in coastal waters  
( $-da/dt$ ) (the pattern that was observed in the EPE from 2019; Fig. 3), results in conservative estimates of SGD induced by  
EPE.

### A.2.4 Endmember selection

Due to the large spatial variability of Ra isotopes in the groundwater activity at the experimental site of Argentona, constraining  
405 the Ra activity of the SGD endmember for both the terrestrial and marine components is particularly difficult. To overcome  
this limitation, we used the activity ratio of  $^{224}\text{Ra}/^{228}\text{Ra}$  measured in the potential groundwater endmembers and the coastal  
ocean, which can help in identifying the most likely endmembers (Diego-Feliu et al., 2021). Endmembers were selected  
according to the following conditions: (1) the selection of the terrestrial Ra endmembers ( $Ra_{TSGD}$ ) was constrained to  
groundwater samples with low salinities ( $\text{Sal} < 5$ ); and (2) the  $^{224}\text{Ra}/^{228}\text{Ra}$  activity ratios of both endmembers must satisfy the  
410 following equation:

$$\frac{{}^{224}\text{Ra}_{TSGD}}{{}^{228}\text{Ra}_{TSGD}} < \frac{F_{Ra224}}{F_{Ra228}} < \frac{{}^{224}\text{Ra}_{MSGD}}{{}^{228}\text{Ra}_{MSGD}}, \quad (\text{A2})$$

where  $F_{Ra-224}/F_{Ra-228}$  is the ratio between the total fluxes of  $^{224}\text{Ra}$  and  $^{228}\text{Ra}$  to the coastal ocean for each of the three  
samplings. A terrestrial and marine SGD was determined for each of any possible combinations between terrestrial and marine  
Ra endmembers that satisfied the above-mentioned conditions, and we reported the final SGD fluxes as the median value and  
415 the interquartile range. Conservative fluxes of nutrients were computed by multiplying the minimum concentrations of  
nutrients within the terrestrial and marine endmembers (discriminated by conditions 1 and 2), and the median ( $\pm$  interquartile  
range) of each SGD component (terrestrial and marine).



## B Darcy's law calculations

The relative significance of EPE in annual SGD estimates derived from the Ra mass balance was compared with Darcy flux estimates ( $Q = -k_h \cdot i$ ). For these calculations, hydraulic conductivity ( $k_h$  [ $\text{m s}^{-1}$ ]) was assumed to be in the order of  $10^{-3} \text{ m s}^{-1}$  (characteristic of clean sands) in the range of local studies (personal communication T. Goyetche and L. Del Val). The hydraulic gradient was determined as the difference between mean sea level (MSL) data and groundwater level data acquired from a CTD diver deployed in a piezometric well at the experimental site of the Argentona ephemeral stream (N3-15, 80 m from the shoreline). Absolute Darcy flux results (Fig. B1) should only be taken as indicative. In fact, the relative variation of Darcy flux during EPE can be used as a proxy for groundwater discharge. Results indicate that the EPE from October 2019, December 2019, and January 2020 represented 2, 4, and 6%, respectively, of the annual groundwater discharge. The relative significance of EPE derived from these calculations is slightly lower than those obtained from the Ra mass balance. This discrepancy can be associated with the different discharge processes that each method captures. Whilst Ra mass balance enables the quantification of processes with different spatiotemporal scales and different compositions of groundwater (e.g., terrestrial groundwater discharge, porewater exchange), Darcy's law only captures the discharge of meteoric or brackish groundwater due to the hydraulic gradient at the shallowest aquifer.

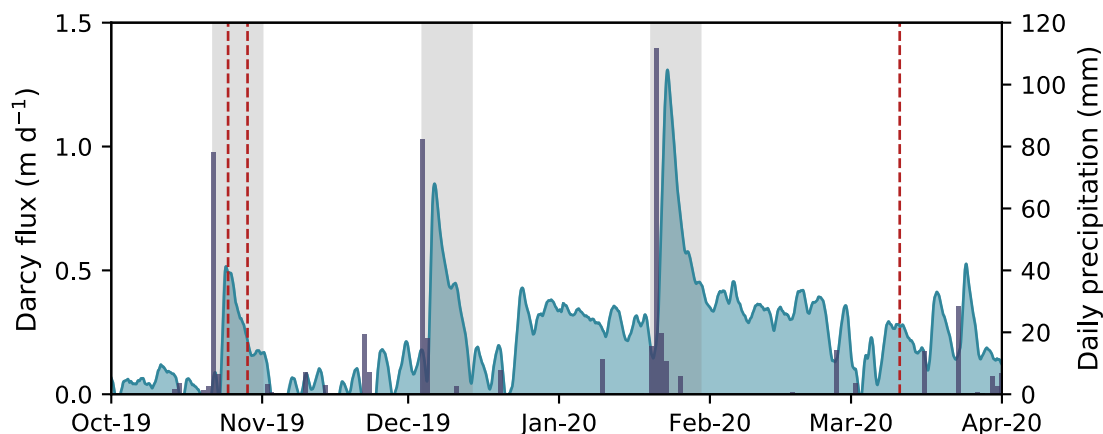


**Figure B1.** Temporal evolution of Darcy flux from October 2019 to April 2020 at the experimental site of the Argentona ephemeral stream. Red lines indicate the groundwater and seawater samplings performed at the study site (P1, P2, and BF) and grey bands indicate the major precipitation events of October 2019, December 2019, and January 2020.

## 7 Acknowledgements

This work was partly funded by the projects PID2019-110212RB-C22, CGL2016-77122-C2-1-R/2-R and PID2019-110311RB-C21 of the Spanish Government and the project TerraMar ACA210/18/00007 of the Catalan Water Agency. The authors want to express their thanks for the support of the Generalitat de Catalunya for MERS (2017 SGR-1588) and GHS



(2017 SGR 1485) for additional funding. The authors would like to thank Maravillas Abad from ICM-CSIC for the analysis of nutrients. M. Diego-Feliu acknowledges the economic support from the FI-2017 fellowships of the Generalitat de Catalunya autonomous government (2017FI\_B\_00365). V. Rodellas acknowledges financial support from the Beatriu de Pinós postdoctoral program of the Generalitat de Catalunya autonomous government (2019-BP-00241). A. Alorda-Kleinglass acknowledges financial support from ICTA “Unit of Excellence” (MinECo, MDM2015-0552-17-1) and PhD fellowship, BES-2017-080740. Albert Folch is a Serra Hunter Fellow. We would like to thank all colleagues from the Grup de Recerca en Radioactivitat Ambiental de Barcelona - GRAB (Universitat Autònoma de Barcelona). We would like to thank SIMMAR (Serveis Integrals de Manteniment del Maresme) and the Consell Comarcal del Maresme for the construction of the research site.

#### 445 **References**

- Adyasari, D., Montiel, D., Mortazavi, B. and Dimova, N.: Storm-Driven Fresh Submarine Groundwater Discharge and Nutrient Fluxes From a Barrier Island, *Front. Mar. Sci.*, 8(July), 1–17, doi:10.3389/fmars.2021.679010, 2021.
- Alorda-Kleinglass, A., Garcia-Orellana, J., Rodellas, V., Cerdà-Domènech, M., Tovar-Sánchez, A., Diego-Feliu, M., Trezzi, G., Sánchez-Quilez, D., Sanchez-Vidal, A. and Canals, M.: Remobilization of dissolved metals from a coastal mine tailing deposit driven by groundwater discharge and porewater exchange, *Sci. Total Environ.*, 688, 1359–1372, doi:10.1016/j.scitotenv.2019.06.224, 2019.
- Alorda-Kleinglass, A., Ruiz-Mallén, I., Diego-Feliu, M., Rodellas, V., Bruach-Menchén, J. M. and Garcia-Orellana, J.: The social implications of Submarine Groundwater Discharge from an Ecosystem Services perspective: A systematic review, *Earth-Science Rev.*, 221, 103742, doi:10.1016/j.earscirev.2021.103742, 2021.
- 455 Anwar, N., Robinson, C. E. and Barry, D. A.: Influence of tides and waves on the fate of nutrients in a nearshore aquifer: Numerical simulations, *Adv. Water Resour.*, 73, 203–213, doi:10.1016/j.advwatres.2014.08.015, 2014.
- Bakhtyar, R., Barry, D. A. and Brovelli, A.: Numerical experiments on interactions between wave motion and variable-density coastal aquifers, *Coast. Eng.*, 60(1), 95–108, doi:10.1016/j.coastaleng.2011.09.001, 2012.
- Beck, A. J. and Cochran, M. A.: Controls on solid-solution partitioning of radium in saturated marine sands, *Mar. Chem.*, 156, 460 38–48, doi:10.1016/j.marchem.2013.01.008, 2013.
- Beck, A. J., Rapaglia, J. P., Cochran, J. K. and Bokuniewicz, H. J.: Radium mass-balance in Jamaica Bay, NY: Evidence for a substantial flux of submarine groundwater, *Mar. Chem.*, 106(3–4), 419–441, doi:10.1016/j.marchem.2007.03.008, 2007.
- Beck, A. J., Rapaglia, J. P., Cochran, J. K., Bokuniewicz, H. J. and Yang, S.: Submarine groundwater discharge to Great South Bay, NY, estimated using Ra isotopes, *Mar. Chem.*, 109(3–4), 279–291, doi:10.1016/j.marchem.2007.07.011, 2008.
- 465 Beusen, A. H. W., Slomp, C. P. and Bouwman, A. F.: Global land-ocean linkage: Direct inputs of nitrogen to coastal waters via submarine groundwater discharge, *Environ. Res. Lett.*, 8(3), doi:10.1088/1748-9326/8/3/034035, 2013.
- Booij, M. J.: Extreme daily precipitation in Western Europe with climate change at appropriate spatial scales, *Int. J. Climatol.*,



- 22(1), 69–85, doi:10.1002/joc.715, 2002.
- 470 Camarasa-Belmonte, A. M. and Segura Beltrán, F.: Flood events in Mediterranean ephemeral streams (ramblas) in Valencia region, Spain, *Catena*, 45(3), 229–249, doi:10.1016/S0341-8162(01)00146-1, 2001.
- Camarasa-Belmonte, A. M. and Soriano-García, J.: Flood risk assessment and mapping in peri-urban Mediterranean environments using hydrogeomorphology. Application to ephemeral streams in the Valencia region (eastern Spain), *Landsc. Urban Plan.*, 104(2), 189–200, doi:10.1016/j.landurbplan.2011.10.009, 2012.
- 475 Camarasa-Belmonte, A. M. and Tilford, K. A.: Rainfall-runoff modelling of ephemeral streams in the Valencia region (eastern Spain), *Hydrol. Process.*, 16(17), 3329–3344, doi:10.1002/hyp.1103, 2002.
- Catalan Water Agency: Model numèric de l'aquífer al·luvial de la riera d'argentina., 2010.
- Charette, M. A.: Hydrologic forcing of submarine groundwater discharge: Insight from a seasonal study of radium isotopes in a groundwater-dominated salt marsh estuary, *Limnol. Oceanogr.*, 52(1), 230–239, doi:10.4319/lo.2007.52.1.0230, 2007.
- 480 Cho, H., Kim, T.-H., Moon, J.-H., Song, B.-C., Hwang, D.-W., Kim, T. and Im, D.-H.: Estimating submarine groundwater discharge in Jeju volcanic island (Korea) during a typhoon (Kong-rey) using humic-fluorescent dissolved organic matter-Si mass balance, *Sci. Rep.*, 11(1), 941, doi:10.1038/s41598-020-79381-0, 2021.
- Cook, P. G., Rodellas, V. and Stieglitz, T. C.: Quantifying Surface Water , Porewater , and Groundwater Interactions Using Tracers : Tracer Fluxes , Water Fluxes , and End-member Concentrations *Water Resources Research*, *Water Resour. Res.*, 54, 2452–2465, doi:10.1002/2017WR021780, 2018.
- 485 Diego-Feliu, M., Rodellas, V., Alorda-Kleinglass, A., Tamborski, J., Beek, P., Heins, L., Bruach, J. M., Arnold, R. and Garcia-Orellana, J.: Guidelines and Limits for the Quantification of Ra Isotopes and Related Radionuclides With the Radium Delayed Coincidence Counter (RaDeCC), *J. Geophys. Res. Ocean.*, 125(4), e2019JC015544, doi:10.1029/2019JC015544, 2020.
- Diego-Feliu, M., Rodellas, V., Saaltink, M. W., Alorda-Kleinglass, A., Goyetche, T., Martínez-Pérez, L., Folch, A. and Garcia-Orellana, J.: New perspectives on the use of  $^{224}\text{Ra}/^{228}\text{Ra}$  and  $^{222}\text{Rn}/^{226}\text{Ra}$  activity ratios in groundwater studies, *J. Hydrol.*, 490 126043, doi:https://doi.org/10.1016/j.jhydrol.2021.126043, 2021.
- Durán, R., Canals, M., Sanz, J. L., Lastras, G., Amblas, D. and Micallef, A.: Morphology and sediment dynamics of the northern Catalan continental shelf, northwestern Mediterranean Sea, *Geomorphology*, 204, 1–20, doi:10.1016/j.geomorph.2012.10.004, 2014.
- 495 Folch, A., del Val, L., Luquot, L., Martínez-Pérez, L., Bellmunt, F., Le Lay, H., Rodellas, V., Ferrer, N., Palacios, A., Fernández, S., Marazuela, M. A., Diego-Feliu, M., Pool, M., Goyetche, T., Ledo, J., Pezard, P., Bour, O., Queralt, P., Marcuello, A., Garcia-Orellana, J., Saaltink, M. W., Vázquez-Suñé, E. and Carrera, J.: Combining fiber optic DTS, cross-hole ERT and time-lapse induction logging to characterize and monitor a coastal aquifer, *J. Hydrol.*, 588, 125050, doi:https://doi.org/10.1016/j.jhydrol.2020.125050, 2020.
- 500 Garcia-Orellana, J., Cochran, J. K., Bokuniewicz, H. J., Daniel, J. W. R., Rodellas, V. and Heilbrun, C.: Evaluation of  $^{224}\text{Ra}$  as a tracer for submarine groundwater discharge in Long Island Sound (NY), *Geochim. Cosmochim. Acta*, 141, 314–330, doi:10.1016/j.gca.2014.05.009, 2014.



- Garcia-Orellana, J., Rodellas, V., Tamborski, J., Diego-Feliu, M., van Beek, P., Weinstein, Y., Charette, M. A., Alorda-Kleinglass, A., Michael, H. A., Stieglitz, T. and Scholten, J.: Radium isotopes as submarine groundwater discharge (SGD) tracers: Review and recommendations, *Earth-Science Rev.*, 103681, doi:10.1016/j.earscirev.2021.103681, 2021.
- 505 Garcia-Solsona, E., Garcia-Orellana, J., Masqué, P. and Dulaiova, H.: Uncertainties associated with <sup>223</sup>Ra and <sup>224</sup>Ra measurements in water via a Delayed Coincidence Counter (RaDeCC), *Mar. Chem.*, 109(3–4), 198–219, doi:10.1016/j.marchem.2007.11.006, 2008.
- Gonneea, M. E., Mulligan, A. E. and Charette, M. A.: Climate-driven sea level anomalies modulate coastal groundwater dynamics and discharge, *Geophys. Res. Lett.*, 40(11), 2701–2706, doi:10.1002/grl.50192, 2013.
- 510 Gwak, Y.-S., Kim, S.-H. S.-W., Lee, Y.-W., Khim, B.-K., Hamm, S.-Y. and Kim, S.-H. S.-W.: Estimation of submarine groundwater discharge in the Il-Gwang watershed using water budget analysis and <sup>222</sup>Rn mass balance, *Hydrol. Process.*, 28(11), 3761–3775, doi:10.1002/hyp.9927, 2014.
- Hu, C., Muller-Karger, F. E. and Swarzenski, P. W.: Hurricanes, submarine groundwater discharge, and Florida’s red tides, *Geophys. Res. Lett.*, 33(11), 2005GL025449, doi:10.1029/2005GL025449, 2006.
- 515 IPCC: Assessment Report 6 Climate Change 2021: The Physical Science Basis, [online] Available from: <https://www.ipcc.ch/report/ar6/wg1/>, 2021.
- Jou-Claus, S., Folch, A. and Garcia-Orellana, J.: Applicability of Landsat 8 thermal infrared sensor for identifying submarine groundwater discharge springs in the Mediterranean Sea basin, *Hydrol. Earth Syst. Sci.*, 25(9), 4789–4805, doi:10.5194/hess-25-4789-2021, 2021.
- 520 Kiro, Y., Weinstein, Y., Starinsky, A. and Yechieli, Y.: The extent of seawater circulation in the aquifer and its role in elemental mass balances: A lesson from the Dead Sea, *Earth Planet. Sci. Lett.*, 394, 146–158, doi:10.1016/j.epsl.2014.03.010, 2014.
- Knee, K. L., Crook, E. D., Hench, J. L., Leichter, J. J. and Paytan, A.: Assessment of Submarine Groundwater Discharge (SGD) as a Source of Dissolved Radium and Nutrients to Moorea (French Polynesia) Coastal Waters, *Estuaries and Coasts*, 39(6), 1651–1668, doi:10.1007/s12237-016-0108-y, 2016.
- 525 Kundzewicz, Z. W. and Döll, P.: Will groundwater ease freshwater stress under climate change?, *Hydrol. Sci. J.*, 54(4), 665–675, doi:10.1623/hysj.54.4.665, 2009.
- Kunkel, K. E., Easterling, D. R., Kristovich, D. A. R., Gleason, B., Stoecker, L. and Smith, R.: Meteorological Causes of the Secular Variations in Observed Extreme Precipitation Events for the Conterminous United States, *J. Hydrometeorol.*, 13(3), 1131–1141, doi:10.1175/JHM-D-11-0108.1, 2012.
- 530 Kwon, E. Y., Kim, G., Primeau, F., Moore, W. S., Cho, H., DeVries, T., Sarmiento, J. L., Charette, M. A. and Cho, Y.: Global estimate of submarine groundwater discharge based on an observationally constrained radium isotope model, *Geophys. Res. Lett.*, 41(23), 8438–8444, doi:10.1002/2014GL061574, 2014.
- Lecher, A. L., Mackey, K., Kudela, R., Ryan, J., Fisher, A., Murray, J. and Paytan, A.: Nutrient loading through submarine groundwater discharge and phytoplankton growth in Monterey bay, CA, *Environ. Sci. Technol.*, 49(11), 6665–6673, doi:10.1021/acs.est.5b00909, 2015.
- 535



- Lee, Y.-W., Kim, G., Lim, W. A. and Hwang, D. W.: A relationship between submarine groundwater-borne nutrients traced by Ra isotopes and the intensity of dinoflagellate red-tides occurring in the southern sea of Korea, *Limnol. Oceanogr.*, 55(1), 1–10, doi:10.4319/lo.2010.55.1.0001, 2010.
- Lionello, P., Bhend, J., Buzzi, A., Della-Marta, P. M., Krichak, S. O., Jansà, A., Maheras, P., Sanna, A., Trigo, I. F. and Trigo, R.: Chapter 6 Cyclones in the Mediterranean region: Climatology and effects on the environment, in *Developments in Earth and Environmental Sciences*, vol. 4, pp. 325–372., 2006.
- Luek, J. L. and Beck, A. J.: Radium budget of the York River estuary (VA, USA) dominated by submarine groundwater discharge with a seasonally variable groundwater end-member, *Mar. Chem.*, 165, 55–65, doi:10.1016/j.marchem.2014.08.001, 2014.
- Luijendijk, E., Gleeson, T. and Moosdorf, N.: Fresh groundwater discharge insignificant for the world’s oceans but important for coastal ecosystems, *Nat. Commun.*, 11(1), doi:10.1038/s41467-020-15064-8, 2020.
- Meenu, S., Gayatri, K., Malap, N., Murugavel, P., Samanta, S. and Prabha, T. V.: The physics of extreme rainfall event: An investigation with multisatellite observations and numerical simulations, *J. Atmos. Solar-Terrestrial Phys.*, 204(January), 105275, doi:10.1016/j.jastp.2020.105275, 2020.
- Van Meter, K. J., Van Cappellen, P. and Basu, N. B.: Legacy nitrogen may prevent achievement of water quality goals in the Gulf of Mexico, *Science (80-. )*, 360(6387), 427–430, doi:10.1126/science.aar4462, 2018.
- Michael, H. A., Mulligan, A. E. and Harvey, C. F.: Seasonal oscillations in water exchange between aquifers and the coastal ocean., *Nature*, 436(7054), 1145–1148, doi:10.1038/nature03935, 2005.
- Michael, H. A., Charette, M. A. and Harvey, C. F.: Patterns and variability of groundwater flow and radium activity at the coast: A case study from Waquoit Bay, Massachusetts, *Mar. Chem.*, 127(1–4), 100–114, doi:10.1016/j.marchem.2011.08.001, 2011.
- Monsen, N. E., Cloern, J. E., Lucas, L. V. and Monismith, S. G.: A comment on the use of flushing time, residence time, and age as transport time scales, *Limnol. Oceanogr.*, 47(5), 1545–1553, doi:10.4319/lo.2002.47.5.1545, 2002.
- Montiel, D., Lamore, A., Stewart, J. and Dimova, N.: Is Submarine Groundwater Discharge (SGD) Important for the Historical Fish Kills and Harmful Algal Bloom Events of Mobile Bay?, *Estuaries and Coasts*, 42(2), 470–493, doi:10.1007/s12237-018-0485-5, 2019.
- Moore, R. J.: The PDM rainfall-runoff model, *Hydrol. Earth Syst. Sci.*, 11(1), 483–499, doi:10.5194/hess-11-483-2007, 2007.
- Moore, W. S.: The subterranean estuary: A reaction zone of ground water and sea water, *Mar. Chem.*, 65(1–2), 111–125, doi:10.1016/S0304-4203(99)00014-6, 1999.
- Moore, W. S.: Ages of continental shelf waters determined from <sup>223</sup>Ra and <sup>224</sup>Ra, *J. Geophys. Res.*, 105(C9), 117–122, doi:10.1029/1999JC000289, 2000.
- Moore, W. S. and Arnold, R.: Ra in coastal waters using a delayed coincidence counter, *J. Geophys. Res.*, 101(C1), 1321, doi:10.1029/95JC03139, 1996.
- Moore, W. S. and Reid, D. F.: Extraction of Radium from Natural Waters Using Manganese-Impregnated Acrylic Fibers, *J.*





- 570 *Geophys. Res.*, 78(36), 8880–8886, doi:10.1029/JC078i036p08880, 1973.  
Moore, W. S. and Wilson, A. M.: Advective flow through the upper continental shelf driven by storms, buoyancy, and submarine groundwater discharge, *Earth Planet. Sci. Lett.*, 235(3–4), 564–576, doi:10.1016/j.epsl.2005.04.043, 2005.  
Palacios, A., Ledo, J. J., Linde, N., Luquot, L., Bellmunt, F., Folch, A., Marcuello, A., Queral, P., Pezard, P. A., Martínez, L., Bosch, D. and Carrera, J.: Time-lapse cross-hole electrical resistivity tomography (CHERT) for monitoring seawater intrusion dynamics in a Mediterranean aquifer, *Hydrol. Earth Syst. Sci. Discuss.*, 1–30, doi:10.5194/hess-2019-408, 2019.
- 575 Pendergrass, A. G. and Knutti, R.: The Uneven Nature of Daily Precipitation and Its Change, *Geophys. Res. Lett.*, 45(21), 11,980–11,988, doi:10.1029/2018GL080298, 2018.  
Rajurkar, M. P., Kothyari, U. C. and Chaube, U. C.: Modeling of the daily rainfall-runoff relationship with artificial neural network, *J. Hydrol.*, 285(1–4), 96–113, doi:10.1016/j.jhydrol.2003.08.011, 2004.
- 580 Ramos, N. F., Folch, A., Fernández-García, D., Lane, M., Thomas, M., Gathenya, J. M., Wara, C., Thomson, P., Custodio, E. and Hope, R.: Evidence of groundwater vulnerability to climate variability and economic growth in coastal Kenya, *J. Hydrol.*, 586(April), 124920, doi:10.1016/j.jhydrol.2020.124920, 2020.  
Robinson, C. E., Xin, P., Santos, I. R., Charette, M. A., Li, L. and Barry, D. A.: Groundwater dynamics in subterranean estuaries of coastal unconfined aquifers: Controls on submarine groundwater discharge and chemical inputs to the ocean, *Adv. Water Resour.*, 115(October 2017), 315–331, doi:10.1016/j.advwatres.2017.10.041, 2018.
- 585 Rodellas, V., Garcia-Orellana, J., Masqué, P., Feldman, M. and Weinstein, Y.: Submarine groundwater discharge as a major source of nutrients to the Mediterranean Sea, *Proc. Natl. Acad. Sci.*, 112(13), 3926–3930, doi:10.1073/pnas.1419049112, 2015.  
Rodellas, V., Garcia-Orellana, J., Trezzi, G., Masqué, P., Stieglitz, T. C., Bokuniewicz, H. J., Cochran, J. K. and Berdalet, E.: Using the radium quartet to quantify submarine groundwater discharge and porewater exchange, *Geochim. Cosmochim. Acta*, 196, 58–73, doi:10.1016/j.gca.2016.09.016, 2017.
- 590 Rodellas, V., Cook, P. G., McCallum, J., Andrisoa, A., Meulé, S. and Stieglitz, T. C.: Temporal variations in porewater fluxes to a coastal lagoon driven by wind waves and changes in lagoon water depths, *J. Hydrol.*, 581, 124363, doi:https://doi.org/10.1016/j.jhydrol.2019.124363, 2020.  
Rodellas, V., Stieglitz, T. C., Tamborski, J., Beck, P. Van, Andrisoa, A. and Cook, P. G.: Conceptual uncertainties in groundwater and porewater fluxes estimated by radon and radium mass balances, , 1–19, doi:10.1002/lno.11678, 2021.
- 595 Rufi-Salis, M., Garcia-Orellana, J., Cantero, G., Castillo, J., Hierro, A., Rieradevall, J. and Bach, J.: Influence of land use changes on submarine groundwater discharge, *Environ. Res. Commun.*, 1(3), 031005, doi:10.1088/2515-7620/ab1695, 2019.  
Santos, I. R., Eyre, B. D. and Huettel, M.: The driving forces of porewater and groundwater flow in permeable coastal sediments: A review, *Estuar. Coast. Shelf Sci.*, 98, 1–15, doi:10.1016/j.ecss.2011.10.024, 2012.
- 600 Santos, I. R., Chen, X., Lecher, A. L., Sawyer, A. H., Moosdorf, N., Rodellas, V., Tamborski, J., Cho, H., Dimova, N., Sugimoto, R., Bonaglia, S., Li, H., Hajati, M.-C. and Li, L.: Submarine groundwater discharge impacts on coastal nutrient biogeochemistry, *Nat. Rev. Earth Environ.*, (March), 108–119, doi:10.1038/s43017-021-00152-0, 2021.  
Sawyer, A. H., Shi, F., Kirby, J. T. and Michael, H. A.: Dynamic response of surface water-groundwater exchange to currents,



- tides, and waves in a shallow estuary, *J. Geophys. Res. Ocean.*, 118(4), 1749–1758, doi:10.1002/jgrc.20154, 2013.
- 605 Schumacher, R. S.: Heavy Rainfall and Flash Flooding, in *Oxford Research Encyclopedia of Natural Hazard Science*, pp. 1–40, Oxford University Press., 2017.
- Spiteri, C., Slomp, C. P., Regnier, P., Meile, C. and Van Cappellen, P.: Modelling the geochemical fate and transport of wastewater-derived phosphorus in contrasting groundwater systems, *J. Contam. Hydrol.*, 92(1–2), 87–108, doi:10.1016/j.jconhyd.2007.01.002, 2007.
- 610 Spiteri, C., Slomp, C. P., Charette, M. A., Tuncay, K. and Meile, C.: Flow and nutrient dynamics in a subterranean estuary (Waquoit Bay, MA, USA): Field data and reactive transport modeling, *Geochim. Cosmochim. Acta*, 72(14), 3398–3412, doi:10.1016/j.gca.2008.04.027, 2008a.
- Spiteri, C., Slomp, C. P., Tuncay, K. and Meile, C.: Modeling biogeochemical processes in subterranean estuaries: Effect of flow dynamics and redox conditions on submarine groundwater discharge of nutrients, *Water Resour. Res.*, 44(2), 1–18, doi:10.1029/2007WR006071, 2008b.
- 615 Stigter, T. Y., Nunes, J. P., Pisani, B., Fakir, Y., Hugman, R., Li, Y., Tomé, S., Ribeiro, L., Samper, J., Oliveira, R., Monteiro, J. P., Silva, A., Tavares, P. C. F., Shapouri, M., Cancela da Fonseca, L. and El Himer, H.: Comparative assessment of climate change and its impacts on three coastal aquifers in the Mediterranean, *Reg. Environ. Chang.*, 14(S1), 41–56, doi:10.1007/s10113-012-0377-3, 2014.
- 620 Sugimoto, R., Honda, H., Kobayashi, S., Takao, Y., Tahara, D., Tominaga, O. and Taniguchi, M.: Seasonal Changes in Submarine Groundwater Discharge and Associated Nutrient Transport into a Tideless Semi-enclosed Embayment (Obama Bay, Japan), *Estuaries and Coasts*, 39(1), 13–26, doi:10.1007/s12237-015-9986-7, 2016.
- Sun, Y. and Torgersen, T.: The effects of water content and Mn-fiber surface conditions on  $^{224}\text{Ra}$  measurement by  $^{220}\text{Rn}$  emanation, *Mar. Chem.*, 62(3–4), 299–306, doi:10.1016/S0304-4203(98)00019-X, 1998.
- 625 Tait, D. R., Erler, D. V., Santos, I. R., Cyronak, T. J., Morgenstern, U. and Eyre, B. D.: The influence of groundwater inputs and age on nutrient dynamics in a coral reef lagoon, *Mar. Chem.*, 166, 36–47, doi:10.1016/j.marchem.2014.08.004, 2014.
- Tamborski, J., Cochran, J. K. and Bokuniewicz, H. J.: Application of  $^{224}\text{Ra}$  and  $^{222}\text{Rn}$  for evaluating seawater residence times in a tidal subterranean estuary, *Mar. Chem.*, 189(January), 32–45, doi:10.1016/j.marchem.2016.12.006, 2017a.
- Tamborski, J., Cochran, J. K. and Bokuniewicz, H. J.: Submarine groundwater discharge driven nitrogen fluxes to Long Island Sound, NY: Terrestrial vs. marine sources, *Geochim. Cosmochim. Acta*, 218, 40–57, doi:10.1016/j.gca.2017.09.003, 2017b.
- 630 Tamborski, J., van Beek, P., Conan, P., Pujo-Pay, M., Odobel, C., Ghiglione, J. F., Seidel, J. L., Arfib, B., Diego-Feliu, M., Garcia-Orellana, J., Szafran, A. and Souhaut, M.: Submarine karstic springs as a source of nutrients and bioactive trace metals for the oligotrophic Northwest Mediterranean Sea, *Sci. Total Environ.*, 732, 1–14, doi:10.1016/j.scitotenv.2020.139106, 2020.
- Taniguchi, M., Dulai, H., Burnett, K. M., Santos, I. R., Sugimoto, R., Stieglitz, T. C., Kim, G., Moosdorf, N. and Burnett, W. C.: Submarine Groundwater Discharge: Updates on Its Measurement Techniques, Geophysical Drivers, Magnitudes, and Effects, *Front. Environ. Sci.*, 7(October), 1–26, doi:10.3389/fenvs.2019.00141, 2019.
- 635 Taylor, R. G., Todd, M. C., Kongola, L., Maurice, L., Nahozya, E., Sanga, H. and MacDonald, A. M.: Evidence of the



- dependence of groundwater resources on extreme rainfall in East Africa, *Nat. Clim. Chang.*, 3(4), 374–378, doi:10.1038/nclimate1731, 2013.
- 640 Uddameri, V., Singaraju, S. and Hernandez, E. A.: Temporal variability of freshwater and pore water recirculation components of submarine groundwater discharges at Baffin Bay, Texas, *Environ. Earth Sci.*, 71(6), 2517–2533, doi:10.1007/s12665-013-2902-1, 2014.
- Valiela, I., Costa, J., Foreman, K., Teal, J. M., Howes, B. and Aubrey, D.: Transport of groundwater-borne nutrients from watersheds and their effects on coastal waters, *Biogeochemistry*, 10(3), 177–197, doi:10.1007/BF00003143, 1990.
- 645 Webster, I. T., Hancock, G. J. and Murray, A. S.: Modelling the effect of salinity on radium desorption from sediments, *Geochim. Cosmochim. Acta*, 59(12), 2469–2476, doi:10.1016/0016-7037(95)00141-7, 1995.
- Werner, A. D., Bakker, M., Post, V. E. A., Vandenbohede, A., Lu, C., Ataie-Ashtiani, B., Simmons, C. T. and Barry, D. A.: Seawater intrusion processes, investigation and management: Recent advances and future challenges, *Adv. Water Resour.*, 51, 3–26, doi:10.1016/j.advwatres.2012.03.004, 2013.
- 650 WHO: Guidelines for Drinking-water Quality 4th Edition. [online] Available from: <http://www.who.int> (Accessed 3 April 2021), 2011.
- Wilson, A. M., Moore, W. S., Joye, S. B., Anderson, J. L. and Schutte, C. A.: Storm-driven groundwater flow in a salt marsh, *Water Resour. Res.*, 47(2), doi:10.1029/2010WR009496, 2011.
- Wilson, A. M., Evans, T. B., Moore, W. S., Schutte, C. A. and Joye, S. B.: What time scales are important for monitoring
- 655 tidally influenced submarine groundwater discharge? Insights from a salt marsh, *Water Resour. Res.*, 51(6), 4198–4207, doi:10.1002/2014WR015984, 2015.
- Yu, X., Xin, P., Lu, C., Robinson, C. E., Li, L. and Barry, D. A.: Effects of episodic rainfall on a subterranean estuary, *Water Resour. Res.*, 53(7), 5774–5787, doi:10.1002/2017WR020809, 2017.
- Zhao, S., Xu, B., Yao, Q., Burnett, W. C., Charette, M. A., Su, R., Lian, E. and Yu, Z.: Nutrient-rich submarine groundwater
- 660 discharge fuels the largest green tide in the world, *Sci. Total Environ.*, 770, 144845, doi:10.1016/j.scitotenv.2020.144845, 2021.